PCCP

Accepted Manuscript

ROYAL SOCIETY OF CHEMISTRY

www.rsc.org/pccp

Pressure-induced phase transition of BiOF: Novel two-dimensional layered structures

Dawei Zhou[a)+], Chunying Pu[a)+], Chaozheng He [a)], Feiwu Zhang[b, c)], Lucheng [a)], BaoGang[d)]

[a)] *College of Physics and Electronic Engineering, Nanyang Normal University, Nanyang 473061, China*

[b)] *Nanochemistry Research Institute, Curtin University, Perth, WA-6845 Australia*

[c)] *State Key Laboratory of Ore Deposit Geochemistry, Institute of Geochemistry,Chinese Academy of Sciences, Guiyang 550002, China*

[d)] *College of Physics and Electronic Information, Inner Mongolia University for the Nationalities, Tongliao 028043, China*

Bismuth oxide haloids BiOXs (X=Cl, Br, I) have become new focused photocatalytic materials after TiO_2 in recently years due to their unique layered structures. Using *ab initio* evolutionary methodology structure search method, we systematically investigate the evolution of BiOF structures under pressure. It is found that BiOF can maintain its layered structure up to 300 GPa. Three stable new phases with *Pnma*, *P*-3*m*1and *Cmcm* structure at pressure of 10, 66, and 286 GPa are identified for the first time. All the newly found phases are two-dimensional layered structures characterized by Bi-O slabs interleaved with F^- anion slabs. Moreover, all three phases are indirect semiconductors with wide band gaps. It is found that pressure can bring great change of the band gaps of BiOF. The band gaps of the high-pressure phases of BiOF vary nearly linearly with pressure but exhibit different pressure trends. The electronic structure, structural stability, phase transition mechanisms and evolution of the Bi-O slabs of BiOF under pressure are discussed.

Keywords: Bismuth oxide haloids; Density functional theory; High phase transition;

I. INTRODUCTION

Layered phase is known to exhibit a lot of exceptional functional properties such as excellent optical and electrical properties. Bismuth oxyhalides (BiOXs, X=Cl, Br, I) are just typical examples, which are one of the most intriguing materials with a variety of technological applications, such as photocatalysts,[1,2] cosmetics,[3] solarcells,[4] photoelectron chemical devices.[5] These compounds attracted much research interest in both experimental and theoretical aspects due to their unique layered two-dimensional (2D) structures. At ambient conditions, BiOXs compounds crystallize into a tetragonal PbFCl-type structure, which is characterized by $[Bi_2O_2]^{2+}$ slabs interleaved by double slabs of halogen anions X^-. The unique layered structure is believed to play an important role in their excellent physical and chemical properties such as anisotropic structural, electrical, and mechanical properties *et al*.[6–8] Especially, the unique layered structure favors the separation of photo-induced electron–hole pairs, thus BiOXs show excellent photocatalytic activity, and a new family of promising photocatalysts is introduced. Up to now, numerous experimental and theoretical studies have focused on the unique layered structures and their excellent photocatalytic activity of BiOXs.[9-18] For instance, the band gap of BiOCl has been determined experimentally to be 3.46[9] or 3.51 eV,[10] while the band gaps of BiOBr and BiOI were evaluated to be 2.91 and 1.92 eV,[10,11] respectively. Nanoparticles of BiOCl, BiOBr, and BiOI also have been synthesized successfully, and BiOI shows a band gap up to 2.96 eV (dependent on the particle size) for nanoparticles.[12] In theory, Zhang *et al.* [9] firstly investigated the electronic structure of BiOCl using the tight-binding linear muffin-tin orbital method. They found that the unique layered structure and indirect optical transition of BiOCl play a crucial role in its excellent photocatalytic activity. Huang *et al.* [13-15]also studied the electronic structures of BiOXs (X=F, Cl, Br, I) with and without Bi 5d states using the first-principles calculations, they found that BiOCl, BiOBr and BiOI crystals have indirect band gaps different from BiOF, and revealed that the involvement of Bi 5d states can expand the band gaps. Using the same method, Zhao *et al.*[16] studied the optical properties of BiOXs crystals. Their calculated

absorption edges were in good agreement with previous experimental results. Recently, Zhang *et al.* [17] studied the facet-dependent photocatalytic properties of BiOXs, and found the X-terminated bulk-like {001} facets result in high thermodynamic stability and efficient separation of photo-induced e^--h^+ pairs. Via density functional theory computations, Zhang *et al.*[18] also investigated the origin of the photocatalytic activities of pure and alloyed BiOXs and compared their photocatalytic properties.

For the famous photocatalytic materials BiOXs with such a unique 2D layered structure, there are many important issues that still remain unsolved. For example, can the unique 2D layered structures of BiOXs exist under high pressure? How do the Bi-O slabs evolve under pressure? What form and characteristics will the Bi-O bonds exhibit under pressure? To address the above issues, we took BiOF as an example and investigated the properties of high-pressure phases of BiOF systematically. We first explored the high-pressure phases of BiOF using the *ab initio* evolutionary methodology, and then investigated the pressure influence on the layered structure of BiOF. The structural stability, electronic structure, and the possible phase transition paths and phase transition mechanism of BiOF under pressure are also discussed in this paper.

II. COMPUTATIONAL METHODS

We carried out a structural search using a global minimization of free energy surfaces using USPEX code,[19-20] which has successfully predicted the ground state structures for a lot of systems.[21–29] The energetic calculations were carried out within the Perdew-Burke-Ernzerhof (PBE) generalized gradient approximation (GGA)[30]as implemented in the VASP code.[31] The electron and core interactions were included by using the frozen-core all-electron projector augmented wave method [32], with Bi：$5d^{10}6s^26p^3$，O: $2s^22p^4$ and F: $2s^22p^5$ treated as the valence electrons. For the structure searches, an energy cutoff of 500 eV and Monkhorst-Pack[33] Brillouin zone sampling grid with the resolution of $2\pi\times0.05$Å^{-1} was used. The most competitive structures were re-optimized more accurately with grids denser than $2\pi\times0.03$ Å^{-1} and energy

cutoff of 800 eV, which ensure that all the enthalpy calculations are well converged to better than 1 meV/atom. Phonon frequencies were calculated using direct supercell method as implemented in the PHONOPY code.[34] The PbFCl to *Cmcm* phase transition was simulated by means of Born–Oppenheimer molecular dynamics (BOMD) as implemented in the CASTEP code.[35] The constant temperature and pressure (NPT) ensemble was adopted. The NPT ensemble was maintained at a constant temperature of 273 K and a pressure of 300 GPa using a Langevin thermostat. A 3×3×2 supercell (72 atoms) of PbFCl phase was used during the molecular dynamic simulations.

III. RESULTS AND DISCUSSIOINS

Structure predictions through the USPEX code with simulation sizes up to 24 atoms/cell were performed at 0 GPa, 50 GPa, 100 GPa, 200 GPa and 300 GPa, respectively. The experimentally observed PbFCl-type structure was successfully reproduced at zero pressure, validating our method adopted here. The final enthalpies of selected BiOF structures are plotted as functions of pressure in Fig. 1. It is found that experimentally observed PbFCl phase remains as the most stable structure up to 10 GPa. After that, *Cm, Amm*2 and *Pnma* phases are found to be energetically more stable than PbFCl phase. Among them, *Pnma* phase is the most stable structure, so we don't discuss *Cm* and *Amm*2 phases in more detail. With increasing pressure up to 66 GPa, a hexagonal *P-3m1* structure is found to be more preferable, which is then replaced by a lower-enthalpy *Cmcm* structure at 286 GPa. The calculated *P-V* curves of BiOF are also shown in the inset of Fig.1.When the three phase transitions occur under pressure, the volume drops are not very large (The volume drops are found to be 1.96, 0.56% and 0.14% for the three phase transitions, respectively, see the inset of Fig.1 in detail). The detailed structural parameters of these newly predicted phases are represented in Table 1. In Fig.2, we also illustrate the supercells of the new predicted structures as well as experimentally observed PbFCl-type structure. Interestingly, all the predicted structures are also 2D layered structures characterized by positively

charged Bi-O slabs interleaved with the F^- slabs, indicating the stability of the 2D layered structure even under high pressure.

In fact, the stability of a structure cannot be determined exclusively by comparing enthalpy. To further check the structural stabilities of the predicted structures, the phonon dispersions of the predicted structures were calculated. As shown in Fig.3, no imaginary phonon frequencies are observed in the whole Brillouin zone, indicating *Pnma*, *P*-3*m*1 and *Cmcm* phases are dynamically stable. From the site-projected phonon density of states (DOS) in Fig.3, it can be seen that the distributions of phonon frequencies for the three predicted phases have nearly the same characteristics. Due to their different atomic masses, the low-energy phonon modes are mainly associated with Bi atoms. The intermediate frequencies correspond to F atoms vibrations, while for the high-energy phonon modes frequencies, O-O vibrations mainly dominate.

As shown in Fig.2, the layered structure of PbFCl phase contains six atoms (2O, 2F, 2Bi), and one O atom is coordinated to four Bi atoms, forming a layer of $[Bi_2O_2]^{2+}$ slabs interleaved by double slabs of halide anion F^-. The internal static electric fields between $[Bi_2O_2]^{2+}$ and the anionic halogen layers were believed to favor the photocatalytic properties of the catalysts. The predicted orthorhombic *Pnma* structure also can be regarded as a layered phase. The configurations of the Bi-O slabs from the top view structures for PbFCl and *Pnma* phases are displayed in Fig. 4a. It can be seen that the Bi-O slabs of PbFCl and *Pnma* phases are very similar, thus we may find the relationship between them simply. As pressure increases, one of the Bi-O bonds (indexed by yellow as shown in Fig.4a) breaks in PbFCl phase, and if the Bi-O slabs in PbFCl phase distort simply, and then we can get the corresponding Bi-O slabs in *Pnma* phase. Thus for *Pnma* phase, one O atom is only bounded with three Bi atoms. The predicted *P*-3*m*1 phase is a hexagonal structure. In this structure, O atoms and Bi atoms form a distorted hexagonal structure with one F^- anion at the center, while other F^- anions lie in the middle of the distorted hexagonal structures. However, the transition from *Pnma* to *P*-3*m*1 is too complex to find the transition path directly. At

higher pressures, *Cmcm* structure becomes stable. It is a layered structure again. We notice that except for the positions of F atoms, the structural characteristics of *Cmcm* phase are nearly the same as that of PbFCl phase. Therefore, we believe PbFCl phase may transform to *Cmcm* phase directly through a metastable process. Interestingly, we reproduced successfully the transition from PbFCl to *Cmcm* by means of NPT molecular dynamics method. In Fig.4b, we illustrated the phase transition process. As pressure increases, there is a relative slip between the two layers of Bi-O slabs, and then the transition from PbFCl to *Cmcm* phase can be achieved. To check the phase transition mechanism, we performed Mulliken populations analysis [36] (shown in Table 2) as implemented in the CASTEP code[32], and compared the bonding situation in PbFCl and *Cmcm* at 300 GPa, more electrons were found to transfer from Bi and O atom to F atom in the *Cmcm* phase, indicating much stronger interactions between the Bi-O slabs and F^- slabs in the *Cmcm* phase. The pressure-induced strong interaction between the Bi-O slabs and F^- slabs is the main cause for phase transition from PbFCl to *Cmcm* phase.

We further examined the pressure dependences of lattice parameters of BiOF, which are shown in Fig.5a. As pressure increases, the lattice parameters of PbFCl phase change rapidly. For *Pnma* phase, only b-axis changes rapidly, a- and c-axis change slowly, indicating a high anisotropy under pressure in this structure. For both *P*-3*m*1 and *Cmcm* phases, the lattice parameters change very slowly with pressure. In Fig.5b, we also show the changes of Bi-O bond lengths with pressure. As we have known, for the three-dimensional Bi_2O_3, one Bi atom is generally coordinated to four, or five, or six O atoms. For PbFCl, *P*-3*m*1and *Cmcm* phases under pressure, one Bi atom is also coordinated to four O atoms. However, for *Pnma* phase, one Bi atom is only coordinated to three O atoms. Moreover, except for the experimentally observed PbFCl phase, the Bi-O bond lengths in the predicted phases are unequal under pressure. The discontinuous changes of the lattice parameters and volumes at the transition points together with the entirely different crystal symmetries in the four structures suggest that the transitions among them are first order.

To investigate the electronic structures of the predicted stable structures, we calculated the band structure and DOSs, and show them in Fig.6. It found that the *Pnma*, *P*-3*m*1, and *Cmcm* phases are all indirect semiconductors characterized by a band gap of 3.41 eV, 2.36 eV, 2.50 eV at 10 GPa, 66 GPa, and 286 GPa, respectively (shown in Figs. 4(a)–4(c)). For PbFCl and *Pnma* phases, the orbitals exhibit apparent flatness in the reciprocal [001] direction (GZ, RX and AM lines for PbFCl, GZ, TY, XU lines for *Pnma*), indicating and the marked localization along the z-axis and the weak interaction between the layers. However, at higher pressures, the orbitals of *P*-3*m*1 and *Cmcm* phases exhibit comparatively large dispersion in the same direction (GA, LM and HK lines for P-3M1, ZT and GY lines for Pnma), implying more strong interaction between the layers at higher pressure.

We further investigate the band gap of BiOF as a function of pressure, which is also shown in Fig.7. As pressure increases, when the three phase transitions happen, there are abrupt changes in the band gaps. For most semiconductors, the band gaps of them usually exhibit a discontinuous change with pressure due to the different atomic arrangements of their high-pressure phases. Furthermore, as pressure increases, the band gaps of PbFCl and *P*-3*m*1 phases increase, while that of *Pnma* and *Cmcm* phases decrease. The different behavior of the band gaps under pressure is helpful for identifying the four phases of BiOF experimentally using an optical measuring device in the further. We notice that both the conduction band minimum (CBM) and the valence band maximum (VBM) of four phases shift to higher energies as pressure increases. For PbFCl and *P*-3*m*1 phases, CBM shifts to higher energies faster, while for *Pnma* and *Cmcm* phases, VBM shifts to higher energies faster. The band gap equals the energy difference between CBM and VBM, so the different behavior of CBM and VBM under pressure will result in a different trend in band-gap pressure coefficient.

We can explain the change of the band gaps with pressure according to an empirical rule reported in the previous work[37-39]. With increasing pressure, the bands with higher total energy (related to principle quantum number *n*) will increase in

energy with respect to lower bands, and the bands with smaller *l* (orbital quantum number *l*) increase in energy with respect to larger *l*. According to the projected density of states, we show the states close to VBM and CBM for different phases in Table 3, which are arranged in a descending order according to their contributions to CBM or VBM. For PbFCl phase, CBM consists mainly of Bi-6p and Bi-6s states with higher *n*, while VBM consists of O-2p and F-2p states with lower *n*, then according to the empirical rule, CBM shifts to higher energies faster than VBM under pressure, thus the band gap of PbFCl increases with pressure. For *Pnma* phase, the contributions from O-2p state with lower n in CBM and Bi-6s state with higher *n* in VBM increase, leading to an increase in the band gap with pressure. At higher pressure, Bi-6s state of CBM in *P*-3*m*1 phase becomes important again, resulting in an increase of the band gap with pressure. While for *Cmcm* phase, compared with the *P*-3*m*1 phase, the increase of Bi-6d state with higher *l* in CBM and Bi-6s state with higher *n* in VBM are responsible for the decrease of the band gap with pressure. So we can see that for BiOF semiconductor, pressure can bring great changes of band gap, providing an effective tool to modify their optical properties.

IV. CONCLUSIONS

In summary, using *ab initio* evolutionary methodology, we explored new high-pressure phases of BiOF up to 300 GPa. Three high-pressure phases were found to be energetically more stable than the experimentally observed PbFCl phase at certain pressure ranges. The unique 2D layered structures found in PbFCl phase are also observed in the three predicted phases. Furthermore, BiOF is found to resist metallization up to 400 GPa, and all the three phases are found to be indirect semiconductors with wide band gap. Moreover, it is found that pressure can bring great change of the band gap of BiOF. The band gaps of the different high-pressure phases of BiOF have a different pressure trend, which is explained according to an empirical rule. It is also found that *CmCm* phase can be obtained directly via a metastable process from ambient-stable PbFCl phase using first principle molecular dynamical simulation. Pressure-induced strong interaction between the Bi-O slabs and

F^- slabs is found to be the main cause for this phase transition. The evolution of the Bi-O slabs under pressure, the possible phase transition paths also discussed in detail. In fact, for other Bismuth oxide haloids, similar phase transitions are also found in our preliminary calculation. Our work will stimulate the future high-pressure experiments on the structural and optical measurements.

References

1 K.L. Zhang, C.M.Liu, F.Q.Huang, C.Zheng, W.D. Wang, Appl. Catal. B, **2006**, 68, 125-129.

2 J.X.Xia, S.Yin, H.M.Li, H.Xu, Y.S.Yan, Q. Zhang, Langmuir, **2011**, 27, 1200-1206.

3 L.Chen, S.F.Yin, R.Huang, Y.Zhou, S.L.Luo, C.T. Au, Catal. Commun., **2012**, 23, 54-57.

4 K.Zhao, Zhang, L.Z.Zhang, Electrochem. Commun., **2009**,11, 612-615.

5 S.H.Cao, C.F.Guo, Y.Lv, Y.J.Guo, Q. Liu, Nanotechnology, **2009**, 20, 275702 -275708

6 Z.T.Deng, D.Chen, B.Peng, F.Q.Tang, Cryst. Growth Des., **2008**, 8, 2995-3303.

7 H.L. Peng, C.K.Chan, S. Meister, X.F.Zhang, Y.Cui, Chem. Mater., **2009**, 21, 247-252.

8 D. Berlincourt, J. Acoust. Soc. Am.,**1992**, 91, 3034-3040.

9 K.L.Zhang, C.M.Liu, F.Q.Huang, C. Zheng, W.D. Wang, Appl. Catal. B, **2006**, 68, 125-129.

10 W.Wang, F.Huang, X.Lin, Scripta Mater., **2007**, 56, 669-672.

11 W.Wang , F.Huang , X.Lin, J.Yang, Catal. Commun., **2008**, 9, 8-12.

12 J.Henle, P.Simon, A.Frenzel, S.Scholz, S.Kaskel, Chem. Mater., **2007**, 19, 366-373.

13 W.L Huang, J. Comput. Chem., **2009**, 30, 1882-1891.

14 W.L.Huang, Q.S.Zhu, Comput. Mater. Sci., **2008**, 43, 1101-1108.

15 W.L.Huang, Q.S.Zhu, J. Comput. Chem., **2009**, 30, 183-190.

16 L.J. Zhao , X.C.Zhang, C.M. Fan, Z.H.Liang, P.D. Han, Physica B, **2012**, 407, 3364-3370.

17 H.J.Zhang, L. Liu, Z.Zhou, RCS Advance, **2012**, **2**, 9224-9229.

18 H.J.Zhang, L.Liu, Z.Zhou, Phys. Chem. Chem. Phys., **2012**, 14, 1286-1292.

19 A. R.Oganov, C.W.Glass, J. Chem. Phys.,**2006**,124, 244704

20 A. R.Oganov, A. O.Lyakhov, M.Valle, Acc. Chem. Res., **2011**,44, 227–237.

21 Q.Zhu, D.Y.Jung, A.R.Oganov, C.W.Glass, C.Gatti, Nature Chemistry, **2013**,5, 61-65

22 S.E.Boulfelfel, Q.Zhu, A.R.Oganov. J. Superhard Mater., **2012**,34, 350-359

23 X.F.Zhou, A.R.Oganov, G.R.Qian, Q.Zhu, Phys. Rev. Lett., **2012,**109, 245503

24 Q.Zhu, Q.Zeng, A.R Oganov, Phys. Rev. B, **2012**, 85, 201407

25 Q.Zhu, A.R.Oganov, M.A.Salvado, P Pertierra, A.O.Lyakhov, Phys. Rev. B, **2011** 83, 193410.

26 X.F.Zhou, X.Dong, A.R.Oganov, Q.Zhu,Y.Tian, Phys. Rev. Lett., **2014**,112, 085502.

27 F.B. Tian, D.F. Duan, D. Li,C.B. Chen, X.J. Sha, Z.L. Zhao,B.B. Liu,and Tian Cui, Sci. Rep., **2014**,4,5759.

28 D.F. Duan, X.L.Huang, C.B. Chen, F.B.Tian, K. Bao, D.Li, Y.X. Liu, H.Y. Yu, B.B. Liu and T.Cui, RSC Advances, **2014**, 4, 32068-32074.

29 D.Li, F.B.Tian, D.F.Duan, K.Bao, B.H.Chu, X.J.Sha, B.B.Liu and **T.Cui**, RSC Advances, **2014**, 4, 10133-10139.

30 J.Perdew, K.Burke, M.Ernzerhof, Phys. Rev. Lett., **1996**, 77, 3865.

31 G. Kresse,J Furthmüller, Phys. Rev. B, **1996**, 54, 11169.

32 P. E. Blöchl,Phys.Rev.B, **1994**, 50, 17953.

33 H. J.Monkhorst, J. D.Pack, Phys.Rev.B, **1976**, 13, 5188.

34 A.Togo, F.Oba, I.Tanaka, Phys. Rev. B, **2008**, 78, 134106.

35 M. D.Segall, P. L. D. Lindan, M. J.Probert, C. J.Pickard, P. J.Hasnip, S. J.Clark, M. C. Payne, J. Phys.: Condens.Matter, **2002**, 14, 2717-2744.

36 R. S. Mulliken, J. Chem. Phys., **1995**, 23,1833–184

37 A. Lazicki, C. W. Yoo,1, W. J. Evans, M. Y. Hu, P. Chow, and W. E. Pickett, Phys. Rev. B,**2008**,78, 155133

38 A. K. McMahan, Physica B+C, **1986**, 139-140, 31

39 A. K. McMahan and R. C. Albers, Phys. Rev. Lett.,**1977**, 198249, 1198

Table and Figure Captions:

Fig.1 Main figures: the enthalpies (relative to the *P*-3*m*1 structure) of selected structures of BiOF. Inset: the volume of the most energetic favorite structures as a function of pressure.

Table1. The unit-cell parameters and atomic positions of the *Pnma*, *P*-3*m*1, and *Cmcm* phases at 10 GPa, 66 GPa, and 286 GPa, respectively.

Fig.2 The crystal structures of BiOF. (a) PbFCl, (b) *Pnma*, (c) *P*-3*m*1, and (d) *Cmcm*. The cyan, purple and red spheres represent F, Bi and O atoms, respectively.

Fig.3 The phonon-dispersion curves and phonon density of states (PDOS) for (a) *Pnma*, (b) *P*-3*m*1, and (c) *Cmcm* at 50 GPa, 150 GPa, and 350 GPa, respectively.

Fig.4 Illustrations of the phase transition paths from PbFCl to *Pnma* phase (a) and PbFCl to *Cmcm* phase (b), respectively. The Bi-O bonds indexed by yellow in the PbFCl phase break, forming the B-O slabs of *Pnma* phase.

Table 2. Mulliken populations in PbFCl and *Cmcm* phases at 300 GPa.

Fig.5 The lattice parameters (a) and Bi-O bond lengths (b) as a function of pressure for different phases of BiOF.

Fig.6 The band structure, and total and partial density of states for PbFCl (a), *Pnma* (b), *P*-3*m*1(c) and *Cmcm* (d) at 0 GPa, 10 GPa, 66 GPa, and 286 GPa, respectively.

Fig.7 Band gaps as a function of pressure for different phases of BiOF.

Table 3. The states close to VBM and CBM for different phases of BiOF arranged in a descending order according to their contributions to CBM and VBM.

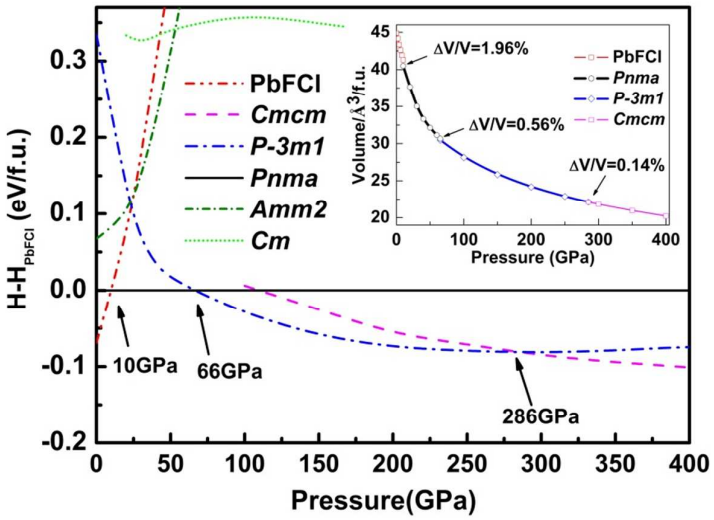

Fig.1

Table1

Space group	Pressure (GPa)	lattice parameters(Å)	Wyckoff positions			
				x	*y*	*z*
Pnma	50	*a*=4.9392	Bi:4c	0.2457	0.2500	0.0894
		b=3.7776	F: 4c	0.0308	0.2500	0.7705
		c=6.8786	O:4c	-0.3131	0.2500	0.0791
P-3*m*1	150	*a*=3.6273	Bi:2d	0.6667	0.3333	0.7349
			F1:1a	0.0000	0.0000	0.0000
		c=4.5338	F2:1b	0.0000	0.0000	0.5000
			O: 2d	0.6666	0.3333	0.1880
Cmcm	350	*a*=3.0471	Bi:4c	0.0000	0.8842	0.2500
		b=8.7839	F: 4c	0.0000	0.5810	0.2500
		c=3.1305	O: 4c	0.0000	0.2481	0.2500

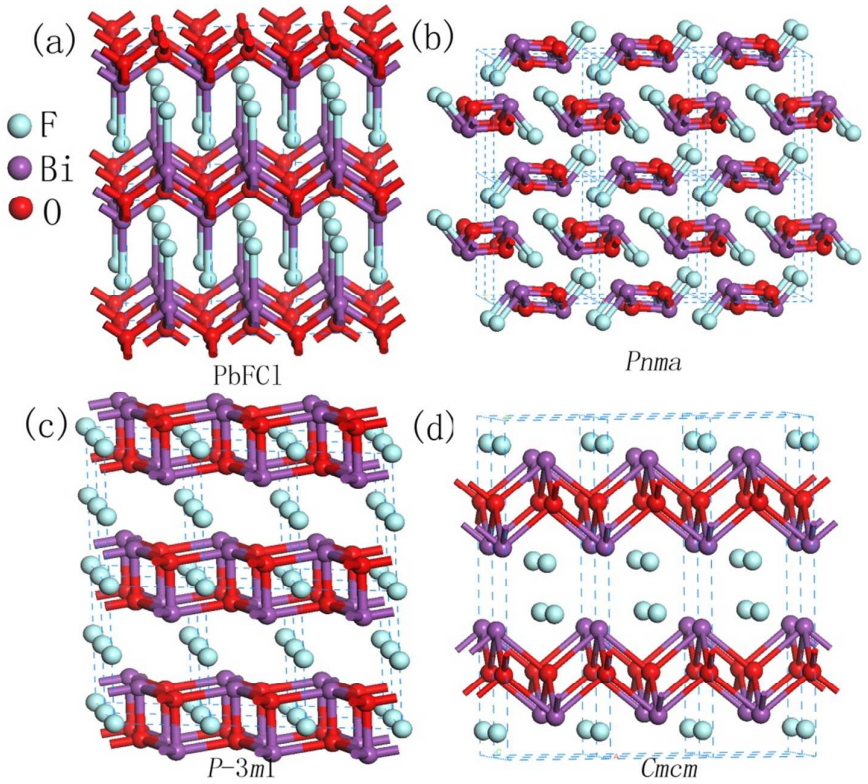

Fig.2

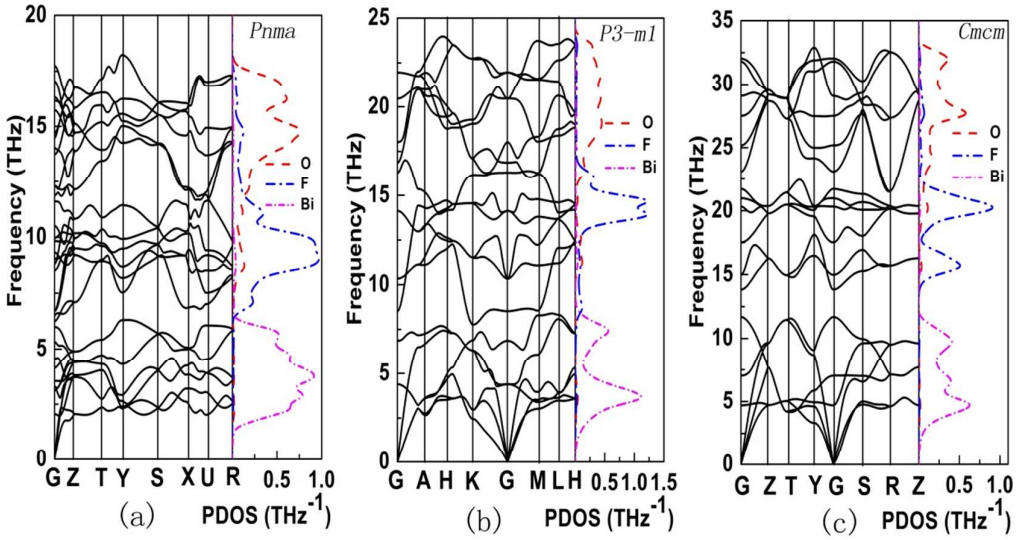

Fig.3

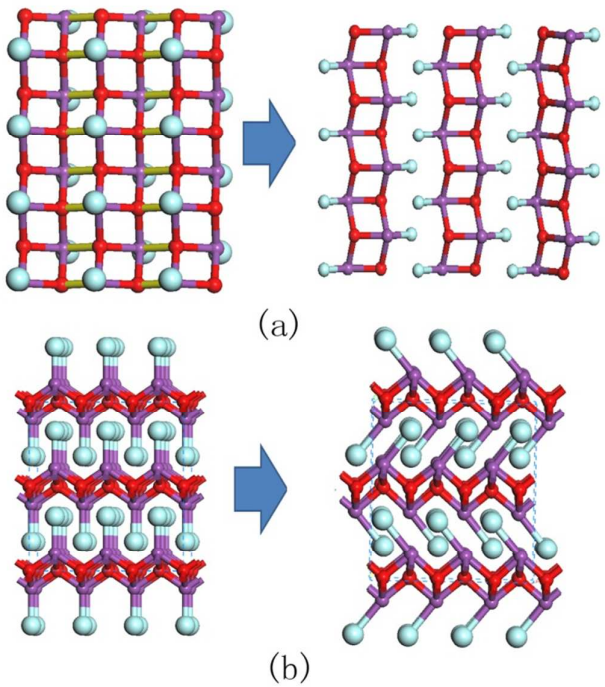

Fig.4

Table 2

Structures	Elements	s(*e*)	p(*e*)	d(*e*)	Total(*e*)	charge(*e*)
PbFCl	O	1.83	5.34	0.00	7.18	-1.18
	F	1.94	5.67	0.00	7.61	-0.61
	Bi	1.87	1.36	9.99	13.21	1.79
Cmcm	O	1.83	5.33	0.00	7.16	-1.16
	F	1.93	5.72	0.00	7.65	-0.65
	Bi	1.78	1.43	9.99	13.19	1.81

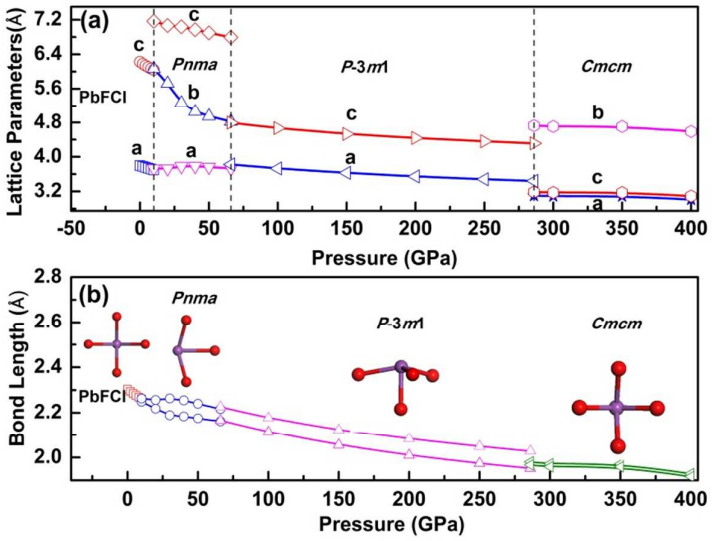

Fig.5

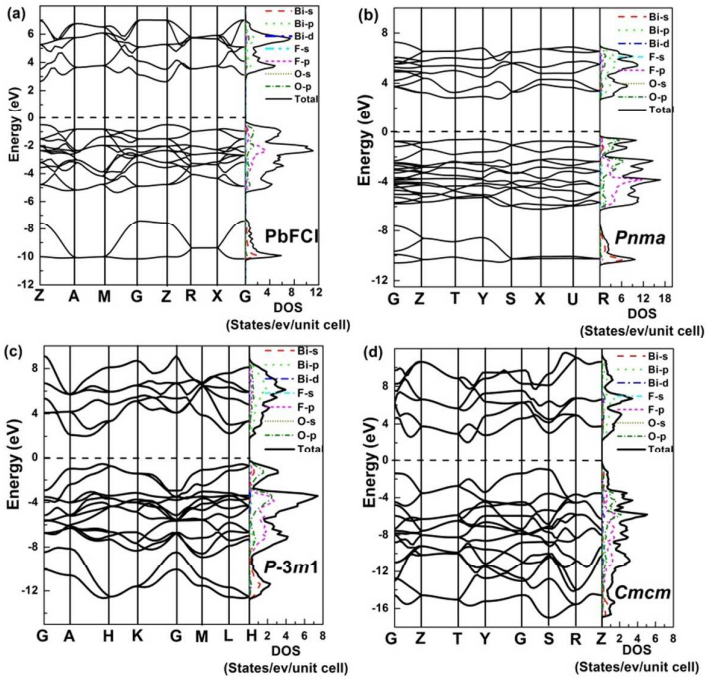

Fig.6

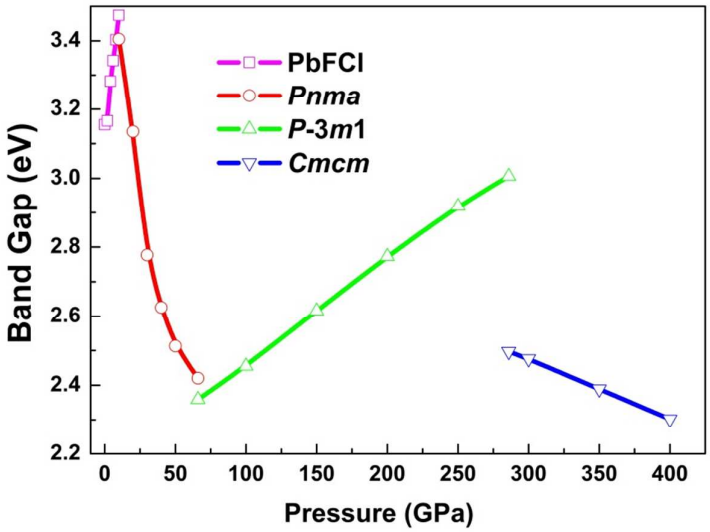

Fig.7

Table 3

	PbFCl	*Pnma*	*P*-3*m*1	*Cmcm*
CBM	*Bi-6p;Bi-6s;O-2p*	*Bi-6p;O-2p;F-2p;*	*Bi-6p;Bi-6s;O-2p;*	*Bi-6p;Bi-6d;O-2p;O-2s;Bi-6s*
VBM	*O-2p;F-2p;Bi-6s;Bi-6p*	*O-2p;Bi-6s;F-2p;Bi-6p*	*O-2p;Bi-6s;F-2p;Bi-6p*	*Bi-6s;O-2p;Bi-6p;F-2p*